RESEARCH PAPER

Solvothermal synthesis of nanocrystalline zinc oxide doped with Mn^{2+}, Ni^{2+}, Co^{2+} and Cr^{3+} ions

Witold Lojkowski · Aharon Gedanken · Ewa Grzanka · Agnieszka Opalinska ·
Tomasz Strachowski · Roman Pielaszek · Anita Tomaszewska-Grzeda ·
Sergyi Yatsunenko · Marek Godlewski · Hubert Matysiak · Krzysztof J. Kurzydłowski

Abstract ZnO nanopowders doped with Mn^{2+}, Ni^{2+}, Co^{2+} and Cr^{3+} ions have been synthesised for the first time using a solvothermal reaction with microwave heating. The nanopowders were produced from a solution of zinc acetate and manganese (II), chromium (III), nickel (II) and cobalt (II) acetates, using ethylene glycol as a solvent. The content of Ni^{2+}, Co^{2+} and Cr^{3+} ions in the solution and in the solid phase were close to each other up to 5 mol%. The doping level of Mn^{2+} ions in the solid is about 50% of that in the solution. No phases or compounds other than ZnO were detected by X-ray diffraction with Mn^{2+}, Co^{2+} and Ni^{2+} doping. With Cr^{3+} ions a small amount of chromium oxide was found. None of the powders displayed any luminescence after doping. The Mn^{2+}-doped powder displayed a paramagnetic behaviour. ESR and magnetisation investigations have revealed that no clustering of Mn^{2+} ions occurred up to a doping level of 3.9 mol%. The average grain size of powders doped with Ni^{2+}, Cr^{3+}, Co^{2+} and Mn^{2+} for a 10 mol% ion content in the solution was about 20 nm and the grain size dispersion 30%. With increasing dopant content the grain size decreased. It appears that the solvothermal process employed allows relatively high doping levels of the transition metal ions to be achieved without any dopant clustering or oxide precipitation.

Keywords Microwave reactor · Zinc oxide · Mn · Co · Cr · Ni · ZnO nanopowder · Solvothermal reaction · Paramagnetism · ESR

W. Lojkowski (✉) · E. Grzanka · A. Opalinska ·
T. Strachowski · R. Pielaszek · A. Tomaszewska-Grzeda
Institute of High Pressure Physics, Polish Academy of
Sciences "Unipress", Sokolowska 29/37, Warsaw 01-142,
Poland
e-mail: wl@unipress.waw.pl

A. Gedanken
Department of Chemistry, Bar-Ilan University,
Ramat-Gan 52900, Israel

S. Yatsunenko · M. Godlewski
Institute of Physics, Polish Academy of Sciences,
Al. Lotnikow 32/46, Warsaw 02-668, Poland

M. Godlewski
Department Mathematics and Natural Sciences College of
Science, Cardinal S. Wyszynski University, Warsaw,
Poland

H. Matysiak · K. J. Kurzydłowski
Faculty of Materials Science and Engineering,
Warsaw University of Technology, Warsaw, Poland

Introduction

The paper reports the synthesis of nanosized ZnO powders doped with Mn^{2+}, Ni^{2+}, Co^{2+} and Cr^{3+} ions for the first time produced by a solvothermal reaction carried out in a microwave reactor. The reactions

were achieved by the decomposition of acetate solutions in ethylene glycol at pressures up to 2 MPa. The term "doped" in this paper is analogous to "alloyed" as the ion content is high. However, the term "doped" is used to stress the intention of adding ions to the host lattice to modify the magnetic or optical properties of the host.

ZnO is a semiconductor of high chemical and thermal stability, with an energy gap of about 3, 5 eV. Due to the large band gap, ZnO efficiently absorbs ultraviolet light and emits blue light. Nanosized ZnO has found application in the production of UV sunscreens but extensive studies are being carried out for its application in optoelectronic and spintronics. Detailed studies have been carried out on the coupling of the magnetic and optical properties of ZnO doped with magnetic ions. ZnO could, according to Dietl et al. (2000), Sharma et al. (2004), Chien et al. (2004), Blythe et al. (2004) and Liu et al. (1992) be one of the materials in which ferromagnetism is expected at room temperature.

Several papers have reported the production of nanosized powders by microwave activation of hydrothermal synthesis (Komarneni et al. 1992; Somiya and Akiba 1999; Komarneni et al. 2000; Palchik et al. 2000; Palchik et al. 2002; Bondioli et al. 2001; Huang et al. 2003; Opalinska et al. 2006). The interest in these methods of synthesis is stimulated by many reports on the accelerated rates of chemical reaction when microwaves are used as the energy source, energy saving and the advantages for producing clean doped nanopowders (Leonelli and Lojkowski 2007). The reasons that microwaves accelerate some chemical reactions is a question of debate (Perreux and Loupy 2001) and direct microwave effects on chemical reactions cannot be excluded. However, the microwave field may lead to local superheating of fluids because part of the fluid is heated whilst not contacting the vapour nucleation sites (Mingos and Baghurst 1991; Mingos 1994; Whittaker and Mingos 1994). Microwave heating is particularly useful for reducing the reaction time in high pressure vessels because the energy is transmitted directly to the reacting fluids and the thermal inertia of the pressure vessel is not an obstacle to rapid heating (Opalinska et al. 2006).

The main methods for the synthesis of nano-ZnO can be divided into two groups: chemical reactions in the gaseous phase and "wet chemistry" reactions.

The reactions in the gaseous phase enable nanopowders to be obtained by the decomposition of organometallic compounds (Jung et al. 1997). The high cost of the precursors and the difficulty of controlling the partial pressures of the components are important barriers for the application of these methods. Their main restriction is the relatively high process temperature compared to that required in the reported solvothermal method.

Chemical reactions in solutions were reviewed by Cushing et al. (2004). The precipitation–calcination route does not require expensive equipment, but the crystallisation temperature of oxide nanopowders is much higher than that in solvo/hydro thermal solutions, and at the high temperatures involved, the nanopowders may start to sinter. Transformation of the precipitated hydroxides into oxides requires calcination, i.e. annealing at temperatures up to 600 °C. Venkataprasad and Deepak dissolved metal acetates in distilled water, evaporated the water at 100 °C and heated the remaining precipitate at 500 and 600 °C for 3 h (Venkataprasad Bhat and Deepak 2005).

Carrying out hydro- or solvothermal reactions to synthesise nanopowders at a sufficiently high pressure avoids the formation of amorphous phases, hydroxides, or unreacted organic salts (Blythe et al. 2004; Leonelli and Lojkowski 2007; Verbiest and Vermang 2007; Ghosh et al. 2004), i.e. a high degree of crystallinity is achieved, without the need for subsequent furnace annealing. The synthesis of high quality ZnO in hydrothermal conditions requires temperatures in the range of 150 °C to 250 °C and pressures of up to 2.5 MPa (Tomaszewska-Grzeda et al. 2006). There was significant interest in attempting to decrease the synthesis pressure by using a solvent other than water.

Numerous works on the synthesis and properties of ZnO powders doped with selected transition metal ions have been published (Liu et al. 1992; Jayakumar et al. 2006; Borges et al. 2007; Xu et al. 2006; Sato and Katayama-Yoshida 2001; Deka and Joy 2007; Jayakumar et al. 2007; Zhou et al. 2004; Liu et al. 2004; Ekambaram 2005; Li and Haneda 2003). ZnO powders doped with Mn^{2+} obtained by two methods have been reported (Joseph et al. 2005), first grinding ZnO and MnO and sintering the solid mixture at 1,200 °C for 12 and 24 h and second by mixing zinc nitrate and manganese acetate in an aqueous medium,

precipitating the hydroxides using NH_4OH as the precipitating agent, and annealing at 500 and 700 °C for 2 h.

Hydrothermal microwave reactions are especially advantageous for obtaining doped nanopowders, as high purity conditions can be achieved in a microwave reactor because the reacting fluids have no contact with the heating elements and they have the ability to achieve the maximum possible degree of powder crystallinity, whilst keeping a small crystallite size, at a lower temperature than is needed for the calcination processes. In a previous paper the magnetic properties of nanometre size ZnO nanopowders doped with Mn^{2+} were discussed (Tomaszewska-Grzeda et al. 2006). Doping ZnO with Ni^{2+} ions has been studied from the point of view of the effect of the addition of Ni^{2+} ions on the catalytic properties of ZnO for the steam reforming of ethanol (Yang et al. 2006). The addition of Ni ions up to 25 mol% may result in a material with strong magnetic properties (Wakamo et al. 2001; Castel et al. 2007). Similarly ZnO doped or alloyed with Cr_2O_3–ZnO was investigated as a catalyst for the synthesis of methanol (Bradford et al. 2003; Ohta et al. 2004) and for its magnetic properties for a doping level up to 5 mol% (Joseph et al. 2006; Li et al. 2007).

The purpose of the work was to show that conducting a microwave reaction under solvothermal conditions makes it possible to obtain single-phase ZnO nanopowders doped to a high level with Mn^{2+}, Ni^{2+}, Co^{2+} and Cr^{3+} ions, without any clustering of the ions. All these ions are commonly used in diluted magnetic semiconductors (DMS).

Experimental methods

Synthesis method

A solid mixture of 5, 10 and 20 mol% of acetates of Mn^{2+}, Ni^{2+}, Co^{2+} and Cr^{3+} in $Zn(CH_3COO)_2$ was dissolved in ethylene glycol (EG). The metal acetates were purchased from Aldrich and used without further purification. The microwave-driven reaction was conducted in a MARS 5 reactor at 280 °C. EG is an excellent absorber of MW radiation and can be easily heated to its boiling point and a superheated liquid may be obtained. The duration of all the reactions was 40 min under a constant pressure of 2 MPa at a

microwave power of 300 W. At the end of the reaction the precipitate was filtered, washed five times with ethanol, centrifuged and dried in vacuum for 24 h. The powders were characterised as described below. Selected powders were annealed at 300 °C in a helium atmosphere and characterised again.

Characterisation methods

The actual content of ions in the powders may not be identical to that in the solutions. Therefore, the chemical composition of the powders was determined by Inductive Coupled Plasma Spectrometry (ICP-Spectroflame, Germany).

Density measurements were carried out using a helium pycnometer (AccuPyc 1330 Micromeritics). This method enabled the density of ZnO nanopowders to be measured with an accuracy of 0.1 g/cm³. The procedure applied for the precise determination of the density of the nanopowders has been described in refs (Opalinska et al. 2006; Lojkowski et al. 2006). The specific surface area was measured by the B.E.T. method using a Gemini Micromeritics instrument. Having the specific surface area, and assuming that all particles were spherical and identical, the average diameter of the particles was calculated. However, there is a parameter, the average chord C, that can be calculated from the specific surface and does not depend on any assumptions on the shape of the material (Kurzydlowski 1995). It is calculated as follows:

$$C = 2/S \cdot \rho, \qquad (1)$$

where S is the specific surface (m²/g) and ρ is the density (g/m³). The value of ρ was assumed to be 5 T/m³. The X-ray diffraction (XRD) patterns were collected in the 2Θ range of 20 to 90° at room temperature, with a step of 0.02° using an X-ray ($CuK_{\alpha1}$) diffractometer (Model Siemens D5000). Based on the XRD patterns the average crystallite size was determined using the Scherrer's formula (Zachariasen 1945) lattice parameters were calculated using the Rietveld refinement implemented in the PowderCell program version 2.3 (Nolze and Kraus 1998). In the case of Mn^{2+} doped powders the Grain Size Distribution (GSD), assuming that the grain size is an equivalent term to crystallite size, and the dispersion of grain sizes were determined using a newly developed method for fine XRD peak analysis

of polydispersed powders (FA XRD) (Opalinska et al. 2006; Lojkowski et al. 2006). This method permits fitting the peaks using an analytical function with an average particle diameter <R> and the dispersion of particle sizes σ as the fitting parameters.

In addition, the GSD of selected samples was measured using transmission electron microscopy (TEM). Specimens were prepared by dispersing the powders in distilled water using an ultrasonic stirrer. A drop of suspension was placed on a copper grid covered with a transparent polymer film, and then dried and coated with carbon. The GSD was obtained from the TEM images using the MicroMeter software (Wejrzanowski et al. 2006; Wejrzanowski and Kurzydlowski 2003). For each sample the projection areas of more than 1,000 particles were analysed. The assumption that the particles were spherical enabled the equivalent diameter of 3D particles to be estimated. The distribution of this parameter and its statistical description (mean value, coefficient of variation, etc.) were calculated.

The morphology of selected powders was studied by means of a LEO 1530 scanning electron microscope.

Photoluminescence (PL) experiments were performed at room temperature using a SM2203 spectrofluorometer with two double built-in monochromators, using a 150 W high pressure Xe lamp as the excitation source, and a R-928 Hamamatsu photomultiplier for detecting the PL.

The magnetic properties of the ZnO:Mn nanopowders were measured with a home-built SQUID (Superconducting Quantum Interference Device) magnetometer and a Bruker 300 X-band electron spin resonance (ESR) apparatus. For the ESR study the samples were mounted in the TE_{012} cavity in a gas flow cryostat working over a wide temperature range from 2 to 300 K using microwave power between 0 and 200 mW.

Results

Figure 1 shows the XRD patterns of the nanopowders for 10 mol% of doping ions in the solution. Only the ZnO phase was found in Mn^{2+}- doped samples, whilst for the other three ions some unidentified peaks were observed. Figure 2 shows the XRD patterns of Mn^{2+}-,
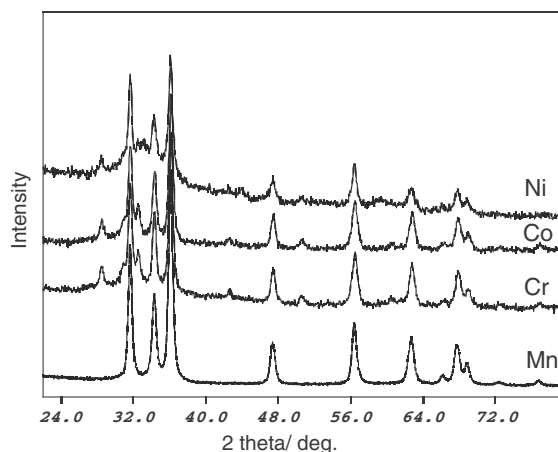
Fig. 1 XRD patterns of nanopowders for 10 mol% of the doping ion in solution. No other phase than ZnO was found in Mn samples
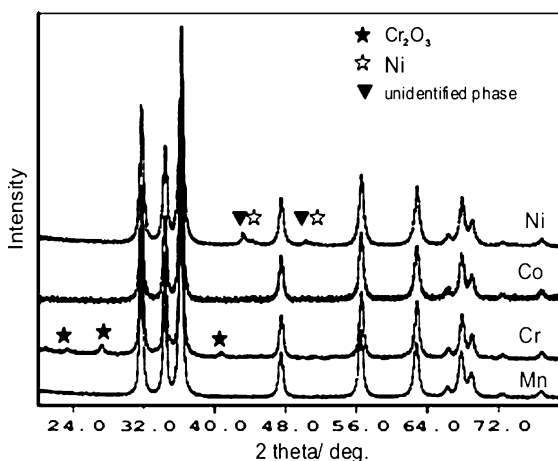
Fig. 2 XRD patterns of Mn^{2+}, Ni^{2+}, Co^{2+} and Cr^{3+}-doped ZnO nanopowders annealed at 300°C in Helium. In the sample with Cr^{3+} traces of Cr_2O_3 were found. In the sample with Ni traces of an unidentified phase were found

Ni^{2+}-, Co^{2+}- and Cr^{3+}-doped ZnO nanopowders annealed at 300 °C under a Helium atmosphere. The unidentified phase in the Ni^{2+}- and Co^{2+}-doped powders had disappeared, and the additional phase in Cr^{3+}-doped powder could be identified as a trace of Cr_2O_3. The XRD peaks attributed to these unwanted phases are indicated by symbols on the XRD pattern.

Table 1 shows the concentrations of Co^{2+}, Ni^{2+}, Cr^{3+} and Mn^{2+} ions in solution and in the nanopowders. A good agreement was found between the composition in the solid and in the solution up to a 5 mol% doping level except in the case of Mn^{2+} ions.

Table 1 Actual metal ion content in the ZnO doped nanopowders

	Dopant content in solution, in mol%			Dopant/ionic radii, nm
	5	10 (9.0 for Mn)	20 (14 for Mn)	
Dopant content in solid in mol%	4.1	8.3	9.9	Cr^{3+}/0.065
	5.0	8.4	15.8	Ni^2/0.078
	5.0	6.1	15.4	Co^{2+}/0.082
	2.6	3.9	7.6	Mn^{2+}/0.091

For the solution concentration of 5 mol% Mn^{2+} the concentration in the solid phase is only 2.6 mol%. For the 10 mol% solution concentrations of Mn^{2+}, Ni^{2+}, Cr^{3+}, and Co^{2+} the amounts found in the solids were 3.9, 8.4, 8.3 and 6.1 mol%, respectively. The largest deviation between the concentration in solution and the actual solid doping level was found for Mn^{2+}.

Tables 2 and 3 present the results of density and specific surface area measurements. Table 2 shows these results for Mn^{2+} at different doping levels and Table 3 shows the results for the same parameters measured for powders with 10 mol% Cr^{3+}, Ni^{2+}, Co^{2+} and Mn^{2+} ions. The density of the powders doped with Mn^{2+} and Co^{2+} ions is close to that of pure ZnO, whereas the powders doped with Ni^{2+} and Cr^{3+} ions display a considerably lower density than pure nano-ZnO. The powders with low densities, are shown to possess a greater surface area.
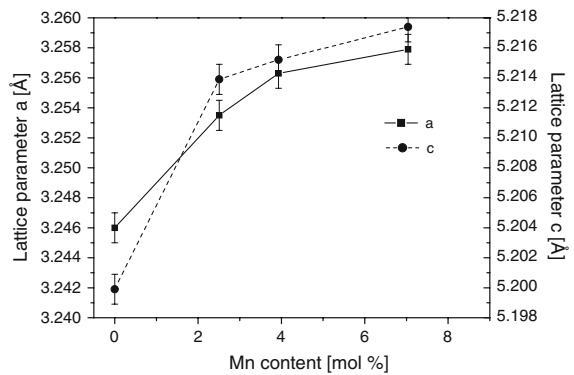
Figure 3 shows the Grain Size Distribution (GSD) for Mn^{2+}-doped powders as a function of the content of Mn ions, assessed by means of FA XRD and measured by means of TEM. The two methods gave very similar results. Table 4 summarises the results

Table 2 Effect of doping level on the specific surface area and density of ZnO and ZnO doped with Mn

Doping level in solution, and in solid phase, mol%	BET, m²/g	Density, g/cm³
0	34	5.1
5/2.6	50	4.3
10/3.9	41	5.0
20/7.6	50	4.7

Table 3 Density and specific surface area of powders synthesised from solutions containing 10 mol% of dopant

Dopant	Real ions content, mol%	Specific surface [m²/g]	Density [g/cm³]
No		34	5.1
Cr^{3+}	6.1	118	3.7
Ni^{2+}	8.3	43	4.4
Co^{2+}	8.4	21	5.3
Mn^{2+}	3.9	41	5.0

Fig. 3 Change of lattice parameters in ZnO doped with Mn as a function of the Mn content in the solid

of grain size calculations based on: specific surface area, the XRD peak width (Scherrer's formula), FA XRD, and TEM image analysis. The GSD dispersion is relatively narrow being in the range of 25%. The results of the assessment of average grain size using three methods: based on Scherrer's formula, on FA XRD method and on TEM image analysis, differed by up to 5 nm i.e. by 25%. Since at present there is no theory enabling preference to be given to one of the above evaluation methods, it seems that this is the limit of accuracy that can be obtained for the determination of the average grain size of nanocrystalline powders with grain sizes in the range of 20 nm.

Figure 4 shows the changes of lattice parameters of ZnO nanopowders doped with Mn^{2+} as a function of the ion content. The lattice constant increased with an increase in the Mn^{2+} concentration; however, a saturation effect was observed.

Table 5 gives the lattice parameters for the nanopowders with 10 mol% dopant in solution and for the undoped ZnO. It can be observed that all

Table 4 Comparison of grain sizes in the nanopowders doped with Mn^{2+} calculated by three different methods. All values in nm

Mn^{2+} content, mol%	Based on specific surface area		Based on XRD		TEM image analysis
	Assuming spherical particles	Average chord	Scherrer's formula	FA XRD	
2.6	28	8	16	21 ± 6	18 ± 5
3.9	29	10	20	24 ± 6	21 ± 6
7.6	26	8	18	23 ± 3	17 ± 4

dopants caused an expansion of the lattice. The degree of lattice expansion is similar for Co, Cr and Ni as the parameter *a* increases by 0.15–0.18% and parameter *c* increases by 0.13–0.15%. For these dopants the ion content in the solution and in the solid was similar. The lattice expansion for Mn^{2+} is much higher than that for the other dopants as the lattice parameters *a* and *c* increased by 0.28 and 0.27%, respectively. For the Mn^{2+} ion, which is larger than the Zn ion, the concentration is lower in the solid than in the solution as shown in Table 1.

The morphology of the powders is presented in Figs. 5 and 6. The SEM images in Fig. 5 show that the particles tended to agglomerate. These agglomerates are formed, either during centrifuging and drying, or during the synthesis process. The formation of the agglomerates was most likely due to van der Waals interactions between the crystallites. The Cr^{3+}- and Ni^{2+}-doped particles displayed a more aggregated form as compared to Co^{2+} and Mn^{2+} doping. The density of the powders was lower for Cr^{3+} and Ni^{2+} doping than for the Co^{2+} and Mn^{2+} doping, and some unidentified phases were observed in the XRD curves (Figs. 1 and 2; Table 3).

The TEM images presented in Fig. 6 show that the particles have an oval shape but some faceting may be observed. A relatively loose structure of the agglomerates powders is seen.

Detailed magnetisation measurements were performed for Mn^{2+}-and Co^{2+}-doped nanopowders. In Fig. 7 the ESR signal of Mn^{2+} ions in powder containing 36 mol% is shown. The spectrum observed consists of one broad featureless signal analogous to the ESR signal of bulk ZnO:Mn with a similar Mn concentration (Wojcik et al. 2006). A characteristic 6-line hyperfine structure of Mn^{2+} ions is not resolved, as expected for samples with a larger Mn content (Furdyna 1982).

Both ESR and SQUID measurements showed paramagnetic responses of the nanopowders with traces of an antiferromagnetic contribution due to the coupling of close Mn ions. The results of magnetisation studies have been described in detail in Tomaszewska-Grzeda et al. 2006.

No PL was observed in the visible part of the spectrum for the doped nanopowders. The absence of PL in these heavily doped samples is believed to be due to the efficient PL deactivation induced by transition metal ions. Such situation has been observed in many other materials, e.g. in ZnS (Yatsunenko et al. in press).

Discussion

Doping or alloying of nanopowders is the subject of extensive research. Doped nanopowders acquire new magnetic or optical properties, depending on the doping ion. Furthermore, the nanoparticles can shield the ion from chemical reactions with the environment. Questions that arise are related to the solubility limits of the doping ions—are they higher or lower in the nanopowders than in the bulk materials and what is the optimum doping level? It is also important to know whether the doping elements segregate on the particle surfaces or are distributed uniformly in the particle, and if in the particle interior, whether they are located interstitially or substitutionally. For materials with a potential for application in spintronics, the coupling between the optical and magnetic properties is of great interest (Dietl et al. 2000). The investigation of these matters requires samples where the dopants do not form clusters as they might influence the magnetic and optical properties.

In a recent paper by the authors it has been shown that hydrothermal synthesis enables high doping levels of aluminium to be achieved in ZnO nanoparticles. In addition, doping with Al^{3+} ions strongly enhances their luminescence (Strachowski et al. 2006). Recent work has also shown that doping of
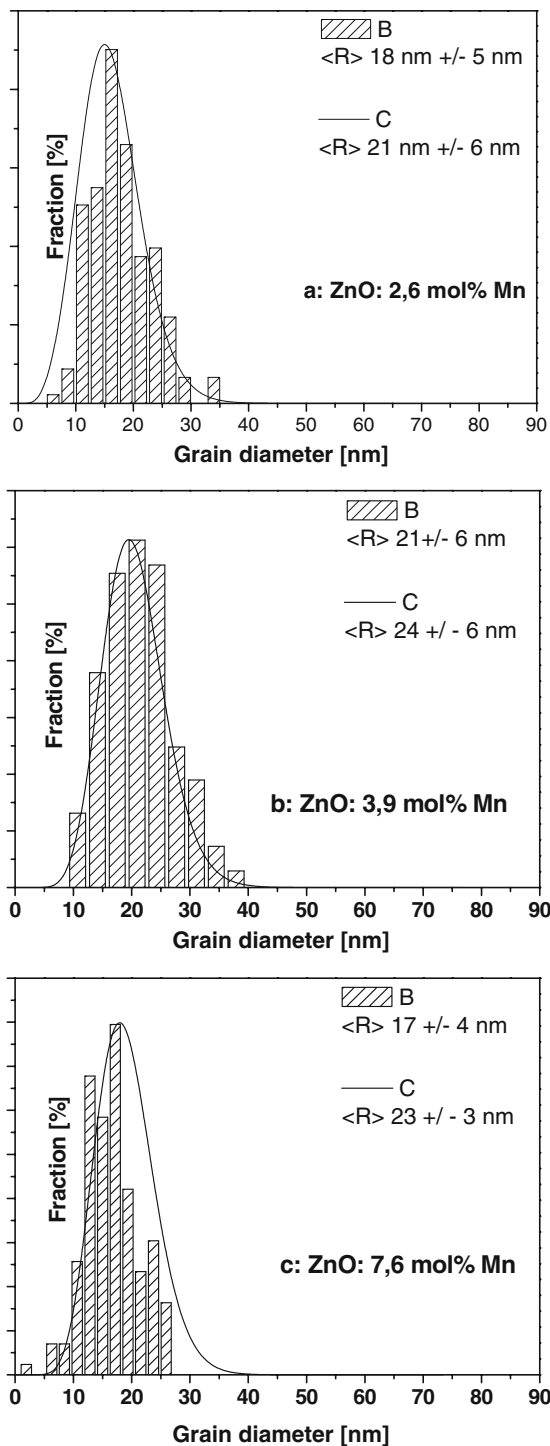
Fig. 4 Grain Size Distribution (GSD) in powders having **a** 2.6 mol%; **b** 3.9 mol% and **c** 7.6 mol% Mn, respectively. Line C: GSD calculated based on Fine Analysis of XRD profiles. Histograms. (B): Results of quantitative analysis of TEM images

ZnO with Mn^{2+} results in powders exhibiting paramagnetic behaviour (Tomaszewska-Grzeda et al. 2006). However, some doping methods used to create nano-ZnO structures produce clusters or metal oxides, which may influence magnetic properties and induce ferromagnetic behaviour (Nolze and Kraus 1998).

From Table 1, which compares the ion contents in the solutions and in the solids, it is seen that for doping with Ni^{2+}, Co^{2+} and Cr^{3+} a large difference is seen only for a 20% dopant content in the solutions. The largest difference is observed for the Mn^{2+} doping. For the concentration of 5 mol% ions, the amount of Co^{2+} and Ni^{2+} in solution and solid is equal, which is an indication of good solubility of these ions in the ZnO lattice. For Cr^{3+} the concentrations in the solution and the solid differ by 1%; however, Cr_2O_3-related peaks were detected in the XRD pattern indicating that a perfect alloy was not formed. With increased levels of doping the ion concentrations in the solids does not grow proportionally to the concentration in the solutions. For a solution concentration of 10%, there is a trend for a decreased amount of ions being incorporated in the particles as the ionic radii increased: Cr^{3+}: 0.065 nm < Ni^{2+}: 0.078 nm < Co^{2+}: 0.082 nm < Zn^{2+}: 0.083 nm < Mn^{2+}: 0.091 nm. For 20% mol in the solution the values for the content in the solid increased further for Ni^{2+} the Co^{2+} cases, was constant for Cr^{3+} and slightly increased in the case of Mn^{2+}. These results are compatible with the formation of a ZnO:MeO alloy, where the solubility limit in the Cr^{3+} case is about 8 mol%. This conclusion is supported by the XRD patterns (Figs. 1 and 2) which reveal no peaks other than those of ZnO phases.

After the synthesis using Cr^{3+} and Ni^{2+} dopants the powders were most likely coated with a layer of hydroxide ions, and the XRD pattern displayed a strong background (Fig. 1). Annealing in helium at 300 °C removed these surface layers (Fig. 2). It is known that the presence of hydroxides leads to an increase in the specific surface area and decrease in the density of the powders as observed in the current study and indicated in Tables 2 and 3 (Opalinska et al. 2006; Lojkowski et al. 2006). The density of Mn^{2+}- and Co^{2+}-doped powders is very close to pure ZnO nanopowders density of ca. 5 g/cm^3, indicating a low level of hydroxides on the surface of the particles. The TEM images do not show any surface layers or a bimodal size distribution of the

Table 5 Lattice constants of the doped ZnO nanopowders synthesised from solutions containing 10 mol% of dopant

Dopant	Real dopant content in solid, mol%	a, A ± 0.001	c, A ± 0.001	Change of parameter "*a*" in %	Change of parameter "*c*" in %
None	0	3.246	5.200	–	–
Cr	8.3	3.251	5.207	0.15	0.13
Ni	8.4	3.251	5.207	0.15	0.13
Co	9.2	3.252	5.208	0.18	0.15
Mn	3.9	3.255	5.214	0.28	0.27

Fig. 5 FE-SEM images of the morphology of nanopowders with 8.3/8.4 mol% of Cr^3/Ni^2
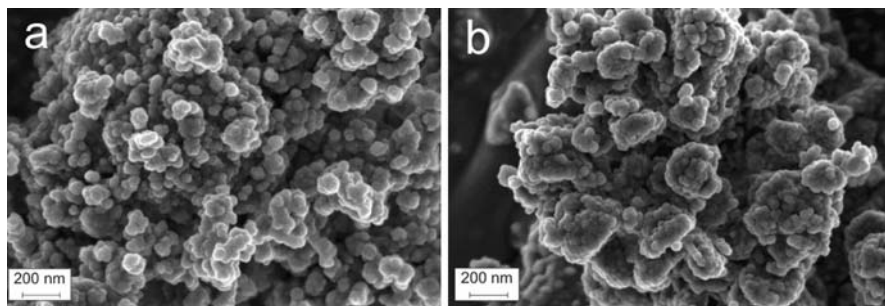
nanoparticles, which might have been an indication of segregation of the dopants or the precipitation of Mn, Ni or Cr oxides.

The observed lattice expansions indicate that the ions used for doping are incorporated into the nanoparticles. The lattice constants increased with increased ion content, but there was a saturation effect. As shown in Table 5, the highest lattice expansion was observed with Mn doping although the Mn^{2+} ions concentration was lowest for the same solution ion content. This is in accord with the large ionic radii of Mn^{2+} giving strong lattice expansion and a low solubility in the lattice. Figure 4 shows the increase of the lattice constants with the increased degree of Mn^{2+} doping. The results are consistent with about 7 mol% of Mn^{2+} ions incorporated in the ZnO lattice, which is close to the solubility limit at 600 °C (Bates et al. 1966).

If all the ions were replacing Zn^{2+} ions, the expansion should be expected only for Mn^{2+}, which has a higher ionic radius than Zn^{2+}. A slight expansion of the lattice for the other ions indicates that they are located interstitially. It is interesting to note that for ZnO:Al nanoparticles the authors observed increased lattice constants despite the Al ions being smaller than the Zn ions indicating the interstitial location of Al ions (Strachowski et al. 2006).

The partial segregation of dopants to the surfaces thereby modifying the surface stress may influence the lattice constants. Changes of lattice constants for surface layers are detected using the Apparent Lattice Parameter (ALP) where the lattice constants determined from each XRD peak are compared (Palosz et al. 2007). However, the use of this method is best suited to very fine particles where the contribution of surfaces to the diffraction pattern is considerable. Gradients of lattice constants between the surface and the interior have been detected for relatively small SiC or diamond nanoparticles about 10 nm in size (Grzanka et al. 2004; Palosz et al. 2006).

The correlations of Mn content with changes of c-axis, a-axis or lattice volume are often observed for thin ZnO:Mn films (Chikoidze et al. 2007). Freestanding ZnO nanopowders are not subjected to external stresses resulting from interactions with the substrate, so changes of lattice constants are connected only with the incorporation of dopant ions in the lattice. This fact opens the chance for determination of the Mn content from the measured lattice constants.

To distinguish between different Mn^{2+} sites in nanopowders it is necessary to observe the ESR signals with the resolved hyperfine structure, as has been detected for Mn^{2+}-doped ZnS nanopowders (Godlewski et al. 2006). This was not possible in this
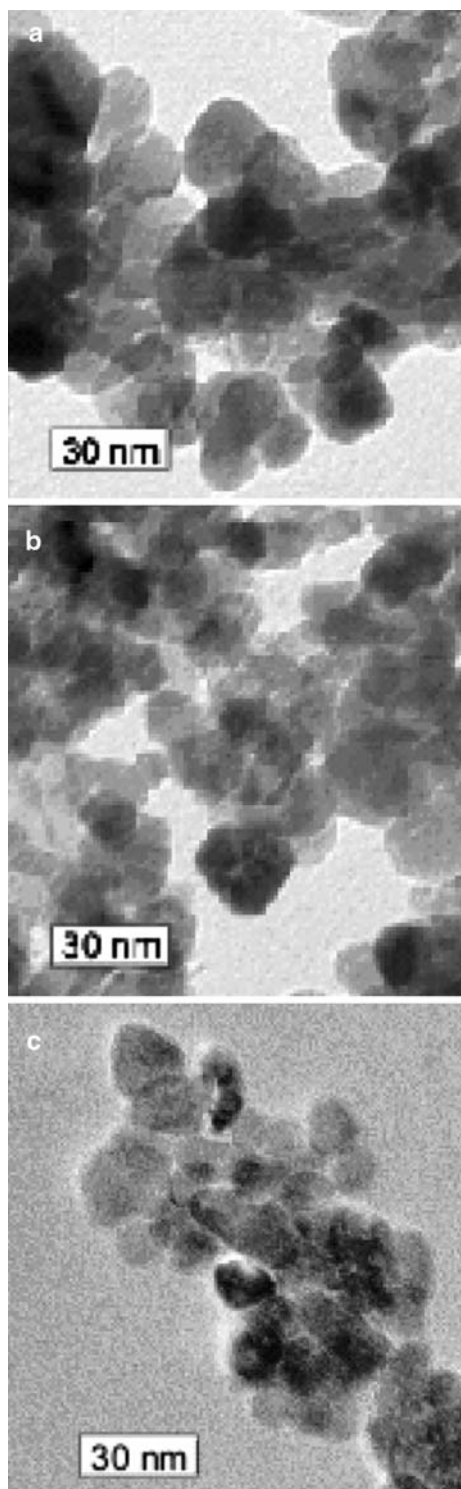
Fig. 6 TEM images of ZnO nanopowders for **a** 8.3 mol% of Cr^{3+} ions, **b** 8.4% mol% of Ni^{2+} and **c** 7.6 mol% of Mn^{2+} ions, respectively
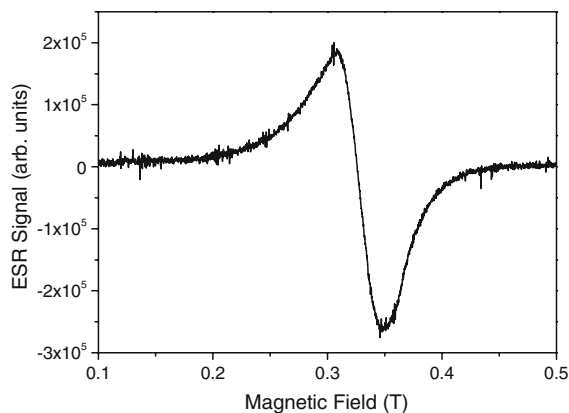
Fig. 7 ESR spectrum of ZnO:Mn with 3.6 mol% concentration measured at liquid helium temperature with an X-band spectrometer

case because the high Mn^{2+} ions concentration leads to the signal being broadened by strong spin–spin interactions between the Mn^{2+} ions. For instance for ZnS:Mn nanopowders (Yatsunenko et al. in press) we observed at the same time three ESR signals of Mn^{2+} ions: one similar to the spectrum reported here, a bulk-like spectrum, and two spectra with a hyperfine structure. In the present case, spectra with hyperfine structure related to Mn^{2+} ions in the atomic layers close to the surface of the nanopowders were not observed. The ESR investigations carried out did not reveal any Mn or Co clustering.

The subject of the location of the doping ions in the present ZnO nanoparticles requires further studies. The current system is particularly interesting in that respect, since the EPR and magnetisation studies indicated that Mn^{2+} did not form clusters and a relatively high solubility of the ions in the lattice was observed.

It was found that solid solutions of CoO–ZnO up to 10 mol% of CoO can be obtained (Pepe et al. 1975). A true solid solution was obtained and Co^{2+} ions replace the Zn^{2+} ions in the tetrahedral positions. The effect of the addition of Co^{2+} was to increase the parameter *a*, in agreement with current work, although this had a higher level of doping of about 15 mol%. A high doping level in the current case is not surprising, since the mutual solubility of ZnO and CoO is high, but the increase of lattice constants may indicate interstitial positioning of some Co^2 ions.

In the case of ZnO:Ni^{2+}, the ICP results indicate that a compound was formed with up to about

8 mol% and lattice expansion occurred (Table 5) so that part of the Ni ions had been incorporated in the lattice. At the same time the solubility of NiO in ZnO is quite low (Bates et al. 1966). However, the XRD patterns revealed some unidentified phases and the SEM images showed strongly aggregated powders (Fig. 5). The present results may indicate that part of the Ni^{2+} ions is incorporated into the lattice and part may be segregated to the surface. The Cr^{2+} doping may follow the same pattern as the Ni^{2+}.

For nanopowders applications a most important parameter is the GSD and the accuracy of determination of the average grain size. The results of several methods of grain size and grain size distribution estimation for Mn^{2+}-doped powder have been compared in this study. Figure 2 and Table 4 show that the average sphere diameter calculated from specific surface clearly gives a diameter a few nanometres larger than that estimated from analysis of the TEM images, Scherrer's formula or Fine Analysis of the shape of the XRD peaks. The average chord is clearly much smaller than the average diameter. The TEM image analysis and both methods based on XRD diffractions gave very similar results with an accuracy of about 5 nm. The FA XRD methods provided results similar to the image analysis for the dispersion, which was about 25%. The general conclusion of these nanometrology exercises is that TEM image analysis and both XRD methods gave comparable results. The narrowest grain distribution corresponded to powders with 2.6 mol% Mn^{2+} content. Furthermore, the various methods to measure particle size lead to different results. The most appropriate method to measure particle size may depend on the physical property that is most important.

In summary, it has been shown for the first time that the solvothermal reaction driven by microwaves has enabled ZnO nanopowders containing Co^{2+}, Ni^{2+}, Cr^{3+} and Mn^{2+} ions to be obtained. Synthesis using solutions containing 5 mol% ions content of Co^{2+}, Ni^{2+} and Cr^{3+} produced an identical amount of ions in the powder particles, but for Mn^{2+} only 2.6 mol% of ions was incorporated into the particles. The amount of ions incorporated for higher solution concentrations did not increase linearly with the concentration.

The presented solvothermal procedure permits the use of a low synthesis temperature compared to that required for gas-phase methods of synthesis thereby preventing any sintering of the particles. The synthesis

pressure in the solvothermal process was 2 MPa, compared to the 2.5–3 MPa pressure used by the authors in the hydrothermal process (Tomaszewska-Grzeda et al. 2006).

The low temperature of the process is probably the reason why no observable clusters of ions or oxides were formed, which is important as clustering is a considerable problem in thin film technology. The fact that no Mn^{2+} clusters are formed is a very different situation to that found in ZnO:Mn films. At temperatures higher than those used in this investigation ions may diffuse or agglomerate to the surface and form clusters which lead to an apparent ferromagnetic powder behaviour.

Conclusions

For the first time ZnO nanopowders doped with Mn^{2+}, Co^{2+}, Cr^{3+} and Ni^{2+} ions have been obtained by solvothermal synthesis in a microwave reactor using acetates as precursors and ethylene glycol as a solvent.

The average grain size of the nanopowders was in the 20 nm range, and the dispersion was about 5 nm. Various methods give results for the average grain size that differed by about 5 nm. The currently used methods to determine grain size and to estimate grain size distribution have therefore an accuracy of about 25% for an average grain size of 20 nm with approximately spherical or oval particles.

For Cr^{3+}- and Ni^{2+}-doped powders, annealing at 300 °C was needed to remove unidentified phases, presumably hydroxides, which remained after synthesis and perturbed measurements of specific surface area and density and caused increased particle agglomeration.

Using Co^{2+} and Ni^{2+} ions, a doping level of up to 15 mol% was achieved, whilst for Mn^{2+} and Cr^{3+} ions up to 7.6 mol% and 10 mol% doping levels, respectively, were obtained.

ESR and magnetisation investigations have shown that there was no formation of Mn^{2+} or Co^{2+} clusters.

The lattice constants increased with the increase of doping level, both for the Mn^{2+} ion, which has a larger ionic radii, and for the other ions with smaller ionic radius than that of Zn^{2+}.

The experiments confirm the high potential offered by solvothermal chemistry in producing oxides with increased dopant concentrations.

References

Bates CH, White WR, Row JR (1966) The solubility of transition metal in zinc oxide and the reflectance spectra of Mn^{+2} and Fe^{+3} in tetrahedral fields. J Inorg Nucl Chem 28:397–405. doi:10.1016/0022-1902(66)80318-4

Blythe HJ, Ibrahim RM, Gehring GA, Neal JR, Fox AM (2004) Mechanical alloying: a route to room-temperature ferromagnetism in bulk $Zn_{1-x}Mn_xO$. J Magn Magn Mater 283:117–127. doi:10.1016/j.jmmm.2004.08.008

Bondioli F, Ferrari AM, Leonelli C, Siligardi C, Pellcani GC (2001) Microwave–hydrothermal synthesis of nanocrystalline Pr-doped zirconia powders at pressure up to 8 MPa. J Am Ceram Soc 84:193–196

Borges RP, Pinto JV, da Silva RC, Goncalves AP, Cruz MM, Godhino M (2007) Ferromagnetism in ZnO doped with Co by ion implantation. J Magn Magn Mater 316:e191–e194. doi:10.1016/j.jmmm.2007.02.109

Bradford MCJ, Konduru MV, Fuentes DX (2003) Preparation, characterization and application of Cr_2O_3/ZnO catalysts for methanol synthesis. Fuel Process Technol 83:11–25. doi:10.1016/S0378-3820(03)00080-8

Castel V, Youssef JB, Brosseau C (2007) Broadband ferromagnetic resonance measurements in Ni/ZnO and Niy-Fe_2O_3 nanocomposites. J Nanomater (Hindawi Publishing Corporation) 27437:16

Chien CH, Chioub SH, Guoaand GY, Yaoc YD (2004) Electronic structure and magnetic moments of 3d transition metal-doped ZnO. J Magn Magn Mater 282:275–278

Chikoidze E, Daumont Y, von Bardleben HJ, Gleize J, Gorochov O (2007) Effect of oxygen annealing on the Mn^{2+} properties in ZnMnO films. J Magn Magn Mater 316:e181–e184. doi:10.1016/j.jmmm.2007.02.083

Cushing BL, Kolesnichenko V, O'Connor CJ (2004) Recent advances in the liquid-phase synthesis of inorganic nanoparticles. Chem Rev 104:3893–3946. doi:10.1021/cr030027b

Deka S, Joy PA (2007) Synthesis and magnetic properties of Mn doped ZnO nanowires. Solid State Commun 142:190–194. doi:10.1016/j.ssc.2007.02.017

Dietl T, Ohno H, Matsukura F, Cibert J, Ferrand D (2000) Zener model description of ferromagnetism in zinc-blende magnetic semiconductors. Science 287:1019–1022. doi:10.1126/science.287.5455.1019

Ekambaram S (2005) Combustion synthesis and characterisation of new class of ZnO-based ceramic pigments. J Alloy Compd 390:L4–L6. doi:10.1016/j.jallcom.2004.08.055

Furdyna JK (1982) Diluted magnetic semiconductors: an interface of semiconductors physics and magnetism. J Appl Phys 53:7637. doi:10.1063/1.330137

Ghosh M, Seshadri R, Rao CNR (2004) A solvothermal route to ZnO and Mn-doped ZnO nanoparticles using the Cupferron complex as the precursor. J Nanosci Nanotechnol 1–2:136–140. doi:10.1166/jnn.2004.021

Godlewski M, Yatsunenko S, Ivanov VY (2006) Recombination processes in nanoparticles of II-Mn-IV compounds—magnetic resonance study. Isr J Chem 46:413–421. doi:10.1560/IJC_46_4_413

Grzanka E, Stelmakh S, Zhao Y, Palosz B, Palosz W (2004) Examination of the atomic pair distribution function (PDF) of SiC nanocrystals by in situ high pressure diffraction. J Alloy Compd 382:133–137. doi:10.1016/j.jallcom.2004.04.142

Huang JR, Xiong ZX, Fang C, Feng BL (2003) Hydrothermal synthesis of $Ba_2Ti_9O_{20}$ nanopowder for microwave ceramics. Mater Sci Eng B99:226–229. doi:10.1016/S0921-5107(02)00541-X

Jayakumar OD, Gopalakrishnan IK, Kulshrestha SK (2006) On the room temperature ferromagnetism of Mn-doped ZnO. Physics B 381:194–198

Jayakumar OD, Gopalkrishnan IK, Sudakar C, Kadam RM, Kulshreshtha SK (2007) Significant enhancement of room temperature ferromagnetism in surfactant coated polycrystalline Mn doped ZnO particles. J Alloy Compd 438:258–262. doi:10.1016/j.jallcom.2006.08.030

Joseph DP, Senthil Kumar G, Venkateswaran C (2005) Structural, magnetic and optical studies of $Zn_{0.95}Mn_{0.05}O$ DMS. Mater Lett 59:2720–2724. doi:10.1016/j.matlet.2005.04.028

Joseph DP, Naveenkumar S, Sivakumar N, Venkatesvaran C (2006) Synthesis of $Zn_{0.95}Cr_{0.05}O$ DMS by co-precipitation and ceramic methods: structural and magnetization studies. Mater Chem Phys 97:188–192. doi:10.1016/j.matchemphys.2005.08.005

Jung KY, Kang YC, Park SB (1997) Photodegradation of trichloroethylene using nanometre-sized ZnO particles prepared by spray pyrolysis. J Mater Sci Lett 16:1848–1849. doi:10.1023/A:1018589206858

Komarneni S, Roy R, Li QH (1992) Microwave–hydrothermal synthesis of ceramic powders. Mater Res Bull 27:1393–1405. doi:10.1016/0025-5408(92)90004-J

Komarneni S, Bruno M, Mariani E (2000) Synthesis of ZnO with and without microwaves. Mater Res Bull 35:1843–1847. doi:10.1016/S0025-5408(00)00385-8

Kurzydłowski KJ (1995) Ralph B The quantitative description of the microstructure of materials. CRC Press, New York

Leonelli C, Lojkowski W (2007) Main development directions in the application of microwave irradiation to the synthesis of nanopowders. Chem Today 25:34–38

Li D, Haneda H (2003) Morphologies of zinc oxide particles and their effects on photocatalysis. Chemosphere 51:129–137. doi:10.1016/S0045-6535(02)00787-7

Li H, Sang JP, Mei F, Ren F, Zhang L, Liu C (2007) Observation of ferromagnetism at room temperature for Cr^+ ions imolanted ZnO thin films. Appl Surf Sci 253:8524–8529. doi:10.1016/j.apsusc.2007.04.028

Liu M, Kitai AH, Mascher P (1992) Point defects and luminescence centres in zinc oxide and zinc oxide doped with manganese. J Lumin 54:35–42. doi:10.1016/0022-2313(92)90047-D

Liu S, Takahashi K, Ueamtsu K, Ayabe M (2004) Hydrogen production by oxidative methanol reforming on Pd/ZnO catalyst: effects of the addition of a third metal component. Appl Catal A 277:265–270. doi:10.1016/j.apcata.2004.09.019

Lojkowski W, Turan R, Proykova A, Morrison M (eds) (2006) Nanometrology report, WWW.nanoforum.org

Mingos DMP (1994) The applications of microwaves in chemistry. Res Chem Intermed 20:85–91. doi:10.1163/156856794X00090

Mingos DMP, Baghurst DR (1991) Applications of microwave dielectric heating effects to synthetic problems in chemistry. Chem Soc Rev 20:1–47. doi:10.1039/cs9912000001

Nolze G, Kraus W (1998) PowderCell 2.0 for windows. Powder Diffr 13:256–259

Ohta M, Ikeda Y, Igarashi A (2004) Preparation and characterization of Pt/ZnO-Cr_2O_3 catalyst for low-temperature dehydrogenation of isobutane. Appl Catal Gen 258:153–158. doi:10.1016/j.apcata.2003.08.021

Opalinska A, Leonelli C, Lojkowski W, Pielaszek R, Grzanka E, Chudoba T, Matysiak H, Wejrzanowski T, Kurzydlowski KJ (2006) Effect of pressure on synthesis of Pr-doped zirconia powders produced by microwave-driven hydrothermal reaction. J Nanomater ID98769:1–8. doi:10.1155/JNM/2006/98769

Palchik O, Zhu Z, Gedanken A (2000) Microwave assisted preparation of binary oxide nanoparticles. J Mater Chem 10:1251–1254. doi:10.1039/a908795h

Palchik O, Gedanken A, Palchik V, Slifkin MA, Weiss AM (2002) Microwave-assisted preparation, morphological, and photoacoustic studies of the Na_4SnSe_4, $K_4Sn_2Se_6$ and $K_4Sn_3Se_8$, Zintl molecular Sn-Se oligomers. J Solid State Chem 165:125–130. doi:10.1006/jssc.2002.9513

Palosz B, Pantea C, Grzanka E, Stelmach S, Proffen T, Zerda TW, Palosz W (2006) Investigation of relaxation of nanodiamond surface in real and reciprocal spaces. Diam Relat Mater 15:1813–1817. doi:10.1016/j.diamond.2006.09.001

Palosz B, Stelmakh S, Grzanka E, Gierlotka S, Palosz W (2007) Application of the apparent lattice parameter to determination of the core-shell structure of nanocrystals. Z Kristallography 222:580–594

Pepe F, Schiavello M, Ferraris G (1975) Characterization of CoO-ZnO. Solid solution. J Solid State Chem 12:63–68. doi:10.1016/0022-4596(75)90178-4

Perreux L, Loupy A (2001) A tentative rationalization of microwave effects in organic synthesis according to the reaction medium and mechanistic considerations. Tetrahedron 57:9199–9223. doi:10.1016/S0040-4020(01)00905-X

Sato K, Katayama-Yoshida H (2001) Ferromagnetism in a transition metal atom doped ZnO. Physica E 10:251–255. doi:10.1016/S1386-9477(01)00093-5

Sharma P, Gupta A, Owens FJ, Inoue A, Rao KV (2004) Room temperature spintronic material—Mn-doped ZnO revisited. J Magn Magn Mater 282:115–121

Somiya S, Akiba T (1999) Hydrothermal zirconia powders: a bibliography. J Eur Ceram Soc 19:81–87. doi:10.1016/S0955-2219(98)00110-1

Strachowski T, Grzanka E, Lojkowski W, Godlewski M, Yatsuenenko S, Presz A, Matysiak H, Piticescu RR,

Monty CJ (2006) Morphology and luminescence properties of zinc oxide nanopowders doped with aluminium ions obtained by hydrothermal and vapor condensation methods. J Appl Phys 89:242102

Tomaszewska-Grzeda A, Opalinska A, Grzanka E, Lojkowski W, Gedanken A, Godlewski M, Yatsunenko S, Osinin V, Story T (2006) Magnetic properties of ZnMnO nanopowders solvothermally grown at low temperature from zinc and manganese acetate. Appl Phys Lett 89:242102. doi:10.1063/1.2404599

Venkaprasad Bhat S, Deepak FL (2005) Tuning the band gap of ZnO by substitution with Mn^{2+}, Co^{2+} and Ni^{2+}. Solid State Commun 135:345–347. doi:10.1016/j.ssc.2005.05.051

Verbiest P, Vermang B (2007) Reactivity of nano zinc metal powder in azo-couplings and in the manufacturing of organozinc halides. Chem Today 25(4):34–38

Wakamo T, Fuijmura N, Morinaga Y, Abe N, Ashida A, Ito T (2001) Magnetic and magneto-transport properties of ZnO:Ni films. Physica E 16:260–264. doi:10.1016/S1386-9477(01)00095-9

Wejrzanowski T, Kurzydlowski KJ (2003) Stereology of grains in nanocrystals. Solid State Phenom 94:221–228

Wejrzanowski T, Pielaszek R, Opalińska A, Matysiak H, Lojkowski W, Kurzydlowski KJ (2006) Quantitative methods for nanopowders characterization. Appl Surf Sci 253:204–208. doi:10.1016/j.apsusc.2006.05.089

Whittaker AG, Mingos DMP (1994) The application of microwave heating to chemical synthesis. J Microw Power Electromagn Energy 29:195–220

Wojcik A, Kopalko K, Godlewski M, Guziewicz E, Jankiela R, Minikayev R, Paszkowicz W (2006) Magnetic properties of ZnMnO films grown at low temperature by atomic layer deposition. Appl Phys Lett 89(051907):3. doi:10.1063/1.2245209

Xu Q, Hartman L, Schmidt H, Hochmut H, Lorenz M, Schmidt-Grund R, Spemann D, Rahm A, Grundman M (2006) Magnetoresistance in pulsed laser deposited 3d transition metal doped ZnO films. Thin Solid Films 515:2549–2554. doi:10.1016/j.tsf.2006.04.024

Yang Y, Ma J, Wu F (2006) Production of hydrogen by steam reforming of ethanol over a Ni/ZnO catalyst. Int J Hydrogen Energy 31:877–882. doi:10.1016/j.ijhydene.2005.06.029

Yatsunenko S, Świątek K, Godlewski M, Fröba M, Klar PJ, Heimbrodt W (2008) Electron spin resonance investigations of ZnMnS nanoparticles. Opt Mater 30:753–755

Zachariasen WH (1945) Theory of X-ray diffraction In crystals. Wiley, New York

Zhou Z, Katoa K, Komakia T, Yoshinoa M, Yukawaa H, Moronnagad M, Moritab K (2004) Effects of dopants and hydrogen on the electrical conductivity of ZnO. J Eur Ceram Soc 24:139. doi:10.1016/S0955-2219(03)00336-4